Nanoscale measurement of the Power Spectral Density of surface roughness: how to solve a difficult experimental challenge

Juan Francisco González Martínez,[*] Inés Nieto Carvajal,[†] José Abad,[‡] and Jaime Colchero Paetz[§]

Universidad de Murcia

(Dated: January 20, 2013)

Abstract

In the present work we show that the correct determination of surface morphology using Scanning Force Microscopy (SFM) imaging and Power Spectral Density (PSD) analysis of the surface roughness is an extremely demanding task that is easily affected by experimental parameters such as scan speed and feedback parameters. We present examples were the measured topography data is significantly influenced by the feedback response of the SFM system and the PSD curves calculated from this experimental data do not correspond to that of the true topography. Instead, either features are "lost" due to low pass filtering or features are "created" due to oscillation of the feedback loop. In order to overcome these serious problems we show that the interaction signal (error signal) can be used not only to quantitatively control but also to significantly improve the quality of the topography raw data used for the PSD analysis. In particular, the calibrated error signal image can be used in combination with the topography image in order to obtain a correct representation of surface morphology ("true" topographic image). From this "true" topographic image a faithful determination of the PSD of surface morphology is possible. The corresponding PSD curve is not affected by the fine-tuning of feedback parameters, and allows for much faster image acquisition speeds without loss information in the PSD curve.

———

[*]Electronic address: jfgm@um.es

[†]Electronic address: inc2@um.es

[‡]Electronic address: jabad@um.es

[§]Electronic address: colchero@um.es

arXiv:1104.4819v2 [cond-mat.mtrl-sci] 27 Jul 2011

1. INTRODUCTION

The nanoscale surface morphology determines a wealth of phenomena which are important for fundamental science as well as for technological applications [1–3]. As is well known, surface roughness is a basic parameter in tribology [4, 5], adhesion phenomena [2, 6], the internal 3–D morphology of nanostructural functional materials [7], wetting properties of surfaces [8–11], optical reflectivity [12, 13] as well as a wealth of biological processes [8, 14]. A precise and reproducible measurement of surface roughness is therefore a key issue for basic science as well as for engineering applications [15]. Accordingly, important efforts have been undertaken in this field ranging from the development of suitable instruments to the normalisation and traceability of length measurements. Traditionally, surface roughness has been measured using profilometers [15, 16], although optical instruments have proven to be very powerful tools as well [17, 18]. With the invention of the Scanning Tunneling Microscope [19] and later, the Scanning Force Microscope (SFM) [20], it has been possible to determine the morphology of surfaces down to the nanometer and even the atomic scale. Accordingly scanning tunneling microscope and scanning force microscope have been widely used for nanoscale roughness characterization [21–23].

The morphology of surfaces can be described using a variety of parameters, the Root Mean Square (RMS) roughness is surely the most common one [24, 25]. In addition, other parameters such as Skewness and Kurtosis can also be used to characterize a surface. Unfortunately, these parameters do not describe the morphology of surfaces in a sufficiently accurate way. This can be understood already on very simple arguments: if we assume that a surface has been discretised using $n \times n$ image points, the whole information content of the surface is reduced to one single value if only the RMS value of the surface is measured. Surfaces with very different morphology – and thus very different behavior with regard to tribology or adhesion – may have the same RMS value of surface roughness. Even worse, it can be shown that for many interesting surfaces the RMS roughness depends on the length scale used for the measurement; that is, as the size of an image is increased, the measured RMS also increases. The RMS-value of surface roughness is therefore not a scale invariant quantity. The precise description of surface morphology therefore calls for more sophisticated tools. As discussed in more detail elsewhere, the Power Spectral Density (PSD) of surface roughness is such a tool [2, 26]. PSD in combination with SFM is an invaluable tool in nanoscale science that should be further developed to really exploit all its possibilities [7, 22, 27–29].

Essentially the PSD describes the mean surface roughness at each length scale in a given image. Typically an image with $n \times n$ points results in a PSD curve with $n/2$ points. Evidently, even

though the reduction of information content is quite high, the reduction is much less as compared to the case where only the RMS is computed. Interestingly, for many surface the roughness varies in a well defined way as the length scale is varied (so-called self afine surfaces). In this case the PSD curve is particularly simple since the relation $\log\left[\text{PSD}(\lambda)\right]$ vs $\log(\lambda)$, where λ is the wavelength of the surface roughness, is linear: $\log\left[\text{PSD}(\lambda)\right]$ vs $\log(\lambda) = s \cdot \log(\lambda) + b$ (see, for example [2]).

From a theoretical point of view, description of surfaces using PSD curves is a very powerful tool and is the basics for modern approaches relating tribology and adhesion phenomena to microscopic and nanoscale properties of surfaces [2]. Unfortunately, experimental determination of nanoscale PSD is quite demanding. Due to the compressing properties of the logarithm a large number of image points are needed to have a significant amount of data points for the horizontal axis ($\log(\lambda)$). Moreover, since the relevant magnitude of the the vertical axis is also logarithmic ($\log\left[\text{PSD}(\lambda)\right]$) a large dynamic range for the height measurement is also required, that is, very large as well as very small height differences have to be acquired equally well. Data adquisition in Scanning Probe Microscopy is sequential and thus inherently slow as compared to other imaging techniques which are generally based on parallel processing (as in most optical microscopes). As is well known, Scanning Probe techniques are based upon a very short range of interaction between the sample to be analyzed and a sharp tip used as probe. In order to obtain surface morphology, the tip is scanned over the sample while a feedback loop is used to keep tip-sample interaction at a constant value. As the tip moves over the sample, this feedback adjusts the (absolute) height of the tip in order to compensate for height variations of the sample surface. Correct adjustment of the feedback parameters is fundamental for the acquisition of good topography raw data: slow feedback will result in "smoothing" of topography data, which would effectively imply low pass filtering and a loss of high frequency roughness, while fast feedback may induce feedback oscillation, creating artificial high frequency roughness not present in the true topography of the sample. Although these feedback issues are always present in SPM experiments and are generally solved in an intuitive way, they are specially relevant if the PSD of surface roughness is determined. Indeed, for its faithful determination each image point of the topography raw data has to be acquired faithfully. For rough surfaces – those for which a PSD analysis is particularly interesting– this is a very difficult experimental challenge: feedback parameters have to be adjusted for fast feedback but avoiding oscillations and the imaging speed has to be chosen to allow correct settling of the feedback at each image point (what is "correct" in this context?). In principle, large enough acquisition times (low acquisition speeds) would allow correct measurement of topographic data; however, for large images (more than $10^3 \times 10^3 =$ a million data points!) this may result in

3

unpractical acquisition times for a single image (up to days!). Moreover, large acquisition times would induce additional problems due to low frequency noise and drift, which would also distort the real topography of the sample [30].

In the present work we will address in detail these issues. We will show that the interaction signal (error signal) can be used not only to quantitatively control but also to significantly improve the quality of the topography raw data used for the PSD analysis. Firstly, we will investigate the effect of feedback response on the determination of the PSD. We will find that, unfortunately, the PSD strongly depends on the setting of the feedback loop (proportional and feedback parameters) as well as on the imaging speed. Secondly, we will show that if the error signal used for the feedback is appropriately calibrated, then the correct determination of the PSD can be significantly improved. In particular, the calibrated error signal can then be used in combination with the topography image for a faithful determination of the surface morphology from which the correct PSD measurement is obtained. Moreover, the corresponding PSD curve is much less affected by a correct fine-tuning of feedback parameters, and allows for much faster image acquisition speeds without loss of information in the PSD curve.

2. EXPERIMENTAL AND DATA PROCESSING

Experiments were performed using a NanoTec SFM system composed of SFM head, high voltage controller and PLL/dynamic measurement board [31]. In this kind of experiments we use sharpened tips with a force constant of 2 N/m and a resonance frequency around 70kHz [32]. In order to obtain maximum stability of the mechanical set-up, the microscope was kept working overnight before the relevant measurements were performed. For the experiments discussed in the present work we operate the Scanning Force Microscope in dynamic mode using the oscillation amplitude as feedback channel (AM-DSFM). Relatively large oscillation amplitudes (50-80 nm peak-peak) and significant reduction of oscillation amplitude are used for feedback (setpoint of 0.5-0.75 a_{free} with a_{free} the free oscillation frequency) are used for feedback. We note that, contrary to typical AM-DSFM operation in air, a phase locked loop within the dynamic measurement board is enabled to keep the tip sample system always at resonance.

As will be discussed in detail elsewhere, we use the thermal noise to precisely calibrate the oscillation amplitude [33]. We have recently shown how the amplitude signal, and in particular the thermal noise of the amplitude signal, is processed by the electronics of a dynamic unit (usually a lock-in scheme together with a phase locked loop to follow the resonance frequency)[34].

4

In order to calibrate de amplitude signal, the dynamic unit is used to demodulate the thermal noise signal which is shifted to $\Delta\nu_A = \nu - \nu_{ref}$ and $\Delta\nu_\Sigma = \nu + \nu_{ref}$ in the "amplitude" and "phase" output of a typical dynamic unit. The corresponding spectrum can then be acquired either with a signal analyser, or from the Fourier transform of the time domain signal of the oscillation amplitude. From the equipartition theorem we obtain $kT/2 = c < a^2 > /2$, where kT is the thermal energy, c the force constant of the cantilever and $< a^2 >$ the square of the rms amplitude signal and from this relation a calibration factor for the oscillation amplitude is obtained. We note that a very low noise level of the detection electronics is needed for this technique to work, since it essentially assumes that all the noise measured is thermal noise. Finally, we also note that a precise calibration of oscillation amplitude (better than 5%) is essential for the work discussed here.

The PSD of an image is usually calculated from the 2–dimensional Fourier Transform of a topographic image by angle averaging the Fourier transform in all directions [2]. Another possibility is to compute the 1–dimensional PSD of each (horizontal) line of an image and then average the power spectrums obtained from all lines of the image. The latter approach is used in the present work and will be discussed in detail elsewhere [30]. PSD curves have been computed using a specifically programmed Mathematica® code or directly within the WSxM® software [10, 35].

3. EFFECT OF FEEDBACK RESPONSE ON THE DETERMINATION OF SURFACE MORPHOLOGY AND POWER SPECTRAL DENSITY OF SURFACE ROUGHNESS

To illustrate the problem of feedback response on the determination of the PSD curve **figure 1** shows a series of topographic images of a glass cover slide. Images were acquired with the same imaging speed (1 line/s) but different proportional/ integral (P/I) feedback parameters. The cover slide has been carefully cleaned in order to remove any contaminations from the surface. We note in this context that already a small number of contamination particles ("nanoscale dust") on the glass surface will change the PSD curve obtained from an experimental image, and thus affect the statistical properties of the measured surface morphology. As discussed in detail elsewhere, a typical glass surface should have a self-affine structure with a fractal dimension $D_f = 1.5$ [2]. Such a fractal surface was considered particularly appropriate for the present study, since it will have surface roughness at all length scales. We recall that an ideal self-affine surface will show a linear relation of the surface roughness in a log-log plot: $\log[\text{PSD}(\lambda)]$ vs $\log(\lambda) = s \cdot \log(\lambda) + b$. For the case of the PSD curves shown (averages of the PSD curves for each line), a fractal dimension

$D_f = 1.5$ should result in a slope $s = 2D_f - 5 = -2$ [2]. In addition, a self-affine surface should present a characteristic disordered appearance having large as well as small scale structures. More precisely, it should have larger (=higher) "large scale structures" and smaller (=lower) "small scale structures". In our experiments, this "cloudy" appearance is best recognised in the insets of the larger topographic images.

Figure 2 shows all PSD curves calculated from the different topographic images shown in **figure 1**. In addition, a master curve is shown for comparison, which gives the "true" PSD, to be discussed in detail below. As expected from the arguments discussed in the introduction, images acquired with different setpoints of the feedback loop indeed result in quite different PSD curves. The PSD curve obtained from the image with the highest P/I values of the feedback loop gives the highest values for the surface roughness. This PSD curve shows three clear peaks, which are only recognised in the PSD curve but not in the corresponding topographic image, where they are essentially imperceptible even in the zooms of the large scale image. As the P/I values are decreased, the measured surface roughness also decreases. The measured curves do not vary in a simple way since the surface roughness is "lost" differently for large and small length scales. In particular, the three peaks observed in the "fasted" image, strongly decrease when the P/I values are decreased. Moreover, the "loss" of surface roughness affects the overall shape of the curve, and in particular its slope, from which the fractal dimension is determined. Finally, we note that the "cleanest" curves with a relatively linear shape are obtained for the lowest values of the P/I parameters. Intuitively we would expect the middle curves to be the better ones because low frequency components are not lost (too much?), and no high frequency components are "produced" due to feedback oscillations. However, how can we assure that this argument is correct? Can we define precise criteria in order to choose the correct PSD-curve? To address this issue, in the next section we will present a simple model in order to relate the measured topography with the true topography and the measured tip-sample interaction. Nevertheless, and in order to stress the importance of this issue, **figure 2** shows a "master curve" representing the true PSD curve of the glass cover slide. This "master curve" will be discussed in detail below. We note that –quite disturbingly– none of the PSD curves obtained from the measured images coincides with the correct (!) "master curve".

4. SIMPLE MODELING OF THE IMAGING ADQUISITION PROCESS

The key idea in the present section is that topography and error signal should be complementary if appropriate measuring units are utilized. Essentially, this is the key point of the present work. Note that if feedback is slow so that small scale features are filtered in the topography image, these features will appear in the signal that is used to maintain a constant tip-sample interaction (error signal). On the contrary, if feedback were perfect –which is unphysical– the interaction signal would be constant and all information would be in the topographic image. Finally, if the feedback oscillates, this oscillation should be visible in both, in the topographic and in the error signal image. In order to analyze this point further, we recall that topography images are acquired by maintaining constant the interaction between tip and sample as the sample is scanned; that is, the feedback should fulfill the mathematical condition

$$I(x, y, z(x, y)) = I_{\text{set}} \tag{1}$$

where I_{set} is the setpoint for the feedback, and $z(x, y)$ is the surface profile followed by the tip. For a given interaction field $I(x, y, z)$, the SPM system therefore "solves" the implicit equation (1) for the surface profile $z(x, y)$. In most cases the force field is complicated and highly non–linear and may even depend on the chemistry of the sample [36]. Then the surface profile depends in a non-trivial way on the set point chosen for image acquisition: $z(x, y) = z(x, y, I_{\text{set}})$. To keep the present analysis simple, we will assume that effects due to non-linearity and surface chemistry are not relevant for the experiments discussed here, that is, we will asume that for a (reasonable) variety of setpoints the measured profile does not depend on the setpoint chosen for the feedback loop.

For a real, non-ideal feedback loop the surface profile $z_{\text{fb}}(x(t))$ followed by the tip of the SFM system will deviate from the true surface by some error profile $\delta z_{\text{err}}(x(t))$:

$$z_{\text{fb}}(x(t)) = z_{\text{true}}(x(t)) + \delta z_{\text{err}}(x(t)) \tag{2}$$

where we have assumed that only the fast scanning direction x is relevant for the present discussion and have thus omitted the slow scan direction y, because for the y direction the feedback loop has sufficient time to settle. In order to keep the notation simple, in what follows we will also omit the time dependence of the signals. Note, however, that this dependence is quite important since a faster scan $x_{\text{fast}}(t)$ will imply more error signal and a different surface profile $z_{\text{fb}}(x_{\text{fast}}(t))$.

For a given surface profile $z_{\text{fb}}(x)$ the interaction signal which is measured will be

$$I_{\text{meas}}(x, z_{\text{fb}}(x)) = I(x, z_{\text{true}}(x) + \delta z_{\text{eff}}(x)) =$$
$$= I(x, z_{\text{true}}(x)) + \frac{\partial I}{\partial z}(x, z_{\text{true}}(x)) \; \delta z_{\text{eff}} + \dots \tag{3}$$
$$\simeq I_{\text{set}} + \Delta I_{\text{err}}(x, z_{\text{true}}(x))$$

where we have kept only linear terms in the expansion of the interaction field $I(x, z)$. In a real experiment, the measured interaction signal I_{meas} therefore deviates from the chosen setpoint I_{set} by the error signal ΔI_{err} defined above. This deviation is caused by a finite feedback response which results in a time lag between the "ideal" height of the tip ($z_{\text{true}}(x)$) and the height which is reached by the feedback loop ($z_{\text{fb}}(x)$). Since the tip moves over the surface, by the time the feedback would have settled to the correct height the tip is at a new (lateral) position $x + \delta x$ where the tip-sample height $z_{\text{true}}(x + \delta x)$ in general will be different and the height $z_{\text{fb}}(x + \delta x)$ found by the feedback loop is, again, not correct. Therefore, a SPM system does not measure the real topography $z_{\text{true}}(x)$, but some other profile $z_{\text{fb}}(x)$. As discussed previously, the amount of error will depend on the scan speed. For linear systems the error is expected to be proportional to the scan speed. An important consequence of relation (3) is that the error profile $\delta z_{\text{eff}}(x)$ can be obtained if the "calibration factor" $\partial I/\partial z$ is known:

$$\delta z_{\text{err}} = \Delta I_{\text{err}}(x)) \Big/ \frac{\partial I}{\partial z}(x, z_{\text{true}}(x)) \tag{4}$$

With this error profile, the true topography can be obtained directly from the measured topography z_{fb} and the error signal ΔI_{err}:

$$z_{\text{true}} = z_{\text{fb}} - \delta z_{\text{err}} =$$
$$= z_{\text{fb}}(x, I_{\text{set}}) - \Delta I_{\text{err}}(x) \Big/ \frac{\partial I}{\partial z}(x, z_{\text{true}}(x)) \tag{5}$$

Unfortunately the slope of the interaction is a quantity which is not easy to determine. Moreover, as discussed above, generally the interaction is non–linear, therefore its slope will vary with tip–sample distance and thus with the set point chosen for constant interaction images. There are, however, two important SFM modes where the interaction signal can be calibrated appropriately and where the error signal depends linearly on tip–sample distance for a suitable range of tip–sample interaction: the normal force signal in the case of contact mode SFM and the oscillation amplitude in the case of the so called AM-DSFM mode. Moreover, in these SFM modes the interaction signal can be calibrated appropriately so that the error signal can be specified directly in length units (nanometers); that is, the interaction signal is then normalised so that conversion

factor $\partial I/\partial z$ is unity, thus $\Delta I_{\mathrm{err}} = \delta z_{\mathrm{err}}$. For contact mode SFM the interaction signal is then essentially the (static deflection) of the cantilever, while in case of AM-DSFM mode the interaction signal is the oscillation amplitude of the cantilever. In these two SFM modes the true topography is directly obtained by simple substraction of the topography and error signal data:

$$z_{\mathrm{true}} = z_{\mathrm{fb}} - \Delta I_{\mathrm{err}} \tag{6}$$

Therefore, from the topographic and the error image the true topography of a sample can be obtained, which is the raw data for the precise determination of the PSD curve. Evidently, the true topography does not depend on the particular set of parameters used for the feedback loop. When the experimentally measured topography and the error signals are considered uncorrelated entities, both will depend in a very strong way on these parameters. Experimentally – as shown in the next section – only the combination of both, topographic and error signal, is therefore a quantity (i.e. the true topography) that does not depend on a particular set of parameters used for data acquisition (proportional/integral parameters, scan speed, etc.).

5. DETERMINATION OF TRUE SURFACE MORPHOLOGY USING TOPOGRAPHIC AND ERROR SIGNAL DATA

To illustrate the issues discussed in the preceding section, **figure 3** shows a series of images of a Platinum film evaporated onto a Silicon surface. Data was acquired in the constant amplitude Dynamic Scanning Force Microscopy mode (also called AM-DSFM). Such a film presents a grain like structure, with a typical lateral grain size of about 50 nm. These Platinum grains can be clearly resolved in the enlarged areas of most images. Topography as well as the corresponding amplitude (=error signal) image are presented. As discussed in the experimental section, the amplitude images have been carefully calibrated in order to determine the precise oscillation amplitude. This allows to show the amplitude images in length units (nm). Therefore all data -topography as well as amplitude images- can be shown with the same units and the same scale, in this case 5 nm. Images have been acquired at a scanning rate of 1 line/s, but with different feedback parameters: the images in the first column have been acquired with the "fastest" feedback (high values for the proportional/integral parameters) while those in the last column have been acquired with the "slowest" feedback parameters. Correspondingly, the Platinum grains are visualised in the topography (top row) when the feedback is "fast", and in the amplitude (middle row) when the feedback is "slow". Note that the first topography image is essentially equivalent to the last amplitude image, that is, visually the contrast of the grains is the same. This proves that the

calibration of the amplitude image is correct, otherwise the height of the grains would appear different in the topography and the amplitude image (recall that the grey scale of the images is the same for all images).

In addition to the topography and error signal images, for each data set PSD curves have been computed for both signals individually as well as for the difference $z_d(x, y) = z_{\text{fb}}(x, y) - a(x, y)$. As expected from the discussion in the previous section, PSD curves obtained from the individual topography and error signal images strongly depend on the feedback parameters. The PSD curves of the difference image give always, within our experimental error, the same "master PSD curve".

Before further discussing the different PSD curves we note that contrary to the case of the glass slide the ("good") PSD curves of the Platinum grains are not linear, instead they saturate for low spacial frequencies (large scales). In order to understand this behaviour, we propose a simple model for the morphology of this surface: a disordered arrangement of individual gaussian grains with a fixed height h_0 and a fixed lateral dimension w_0,

$$z_{Pt}(x, y) = h_0 \, e^{-(x^2+y^2)/(2w_0^2)}$$

In our case, this assumption is not based on any profound insight on the sample, we have chosen this shape because it is smooth on the top and on the bottom of the grains [37] and because its Fourier Transform is directly evaluated,

$$FT\,[z_{Pt}]\,(k_x, k_y) = \frac{1}{2\pi} \int \int dxdy \; e^{\imath(k_x x + k_y y)} \; z_{Pt}(x, y) = \frac{h_0}{\kappa_0^2} \; e^{-(k_x^2+k_y^2)/(2\kappa_0^2)}$$

where $k_i = 1/\lambda_i$ is the spatial frequency in each direction ($i = x$ or y), and $\kappa_0 = 1/w_0$ is the spatial frequency associated to the width of the grains. For a disordered array of N grains we expect an "incoherent" contribution of each grain to the total PSD, and if the grains cover the surface in a dense arrangement, we expect about one grain in a cell of width $2w_0$, therefore the total number of grains is $N \simeq (\text{Scan Size}/2w_0)^2 = \text{Area}/(4w_0^2)$. The curve $\log[\text{PSD}(1/\lambda)]$ vs $\log(1/\lambda)$ should therefore show a flat region for small spacial frequencies up to the frequency $1/w_0$ corresponding to the width of the grains, and a decrease for higher frequencies. Since e^{-x^2} decreases faster than any (inverse) power, this decrease is non-linear, that is, the magnitude of the slope of the $\log[\text{PSD}(1/\lambda)]$ vs $\log(1/\lambda)$ curve increases for high frequencies. Correspondingly, this surface is not self-similar and the notion of fractal dimension is not defined.

This simple model correctly describes the "good" PSD curves shown in **figures 3** and **4**. Moreover, with this simple model for the surface morphology the behaviour of the topographic and amplitude images can be further analysed. In this context we recall that spatial (k) and

temporal frequencies (ν) are related through the scan speed v:

$$k = \frac{1}{v}\,\nu \tag{7}$$

In the graphs shown, the highest and lowest spatial frequencies (0.04 μm^{-1} and 20 μm^{-1}) correspond to a temporal frequency of 1 kHz and 2 Hz.

A characteristic feature of the amplitude PSD curves shown in **figure 3** is that for low spatial frequencies, all curves have a constant slope $s = 2.0 \pm 0.1$. Since for these spatial frequencies the PSD curve of the true topography is constant, we conclude that the slope of the PSD curve is determined by the filtering properties of the feedback loop. Indeed, if the P/I controller is modelled by a simple first order electronic circuit with characteristic time τ_0 we expect transfer functions

$$g_{\text{topo}}\left(\nu\right) = \frac{1}{1 + i\tau_0\nu} \text{ and } g_{\text{amp}}\left(\nu\right) = 1 - g_{\text{topo}}\left(\nu\right) = \frac{i\tau_0\nu}{1 + i\tau_0\nu} \tag{8}$$

for the topographic and the amplitude signals. Therefore, for low frequencies the amplitude signal will grow linearly with frequency up to the characteristic frequency $1/\tau_0$. The power of the amplitude signal increases quadratic with frequency and the $\log\left[\text{PSD}[\text{amplitude}(1/\lambda)]\right]$ vs $\log(1/\lambda)$ curve should give a straight line with slope $s = 2$, as is indeed observed experimentally.

For this sample with constant PSD of surface roughness up to the characteristic spatial frequency $\kappa_0 = 1/w_0$ the PSD of the amplitude signal is therefore easily understood taking into account the transfer function of the feedback loop. A similar analysis for the topographic signal is less evident, because in the frequency range where the topographic signal is filtered (for high frequencies) the PSD curve of the true surface roughness does not follow a simple relation (constant or linear). Nevertheless, as the P/I values are decreased, the topographic signal is clearly filtered more strongly. Moreover, as the P/I values are decreased for the different set of images, the characteristic frequency $1/\tau_0$ of the feedback loop also decreases (spatial frequencies 12.2, 12.2, 8.7, 5, 2.3 nm^{-1} for P/I 90/45, 45/22.5, 15/7.5, 5/2.5, 1/0.5 respectively in **figure 4**). Finally we note that even though topographic and amplitude PSD curves are quite different for each set P/I values, the PSD curves of the difference image give always, within our experimental error, the same "master PSD curve". This is recognised most easily in **figure 4**, where all PSD curves corresponding to the same kind of data (topography, amplitude and difference data) have been collected in the same graph in order to directly visualize how these curves vary as the P/I values are changed. Very clearly the topographic and amplitude signals vary, but the difference signal is constant. We stress that what seems to be a single curve in **figure 4** is the superposition of the five sets of difference data obtained from topographic and amplitude data shown in **figure 3**.

Figure 5 shows a similar data set as that shown in **figure** 3, however in this experiment instead of varying the P/I values, the scan speed is varied (from left to right: 0.5, 1, 2, 4, 8 lines/s). We first note that as the scan speed is increased, a characteristic peak moves towards lower frequencies. This peak is first observed in the second graph [38], and also in the data of **figure** 3 at essentially the same position. We attribute this peak to oscillation of our system rather than to a true topographic feature. Therefore, according to relation (7) as the scan speed is increased, higher temporal frequencies are measured and the (relative) position of the peak shifts towards lower values.

As compared to the data shown in **figure** 3, only the first two data sets give "nice" PSD curves. For high scan speed, the topography and amplitude images do neither result in "clean" PSD curves, nor does the difference data obtained from each set of images result in a PSD curve that is independent of scan speed; that is, the difference PSD curves do not lay on a single "master curve". In the case of the images shown in **figure** 5 we find that data which corresponds to frequencies higher that the peak shows a behaviour which is not compatible with the simple first order model of the feedback loop discussed above. This model essentially predicts a well defined distribution of topographic and amplitude signal as a function of frequency according to relation (8). In particular, the PSD curves of the topographic data acquired at the faster frequencies do not decrease more strongly than the amplitude data, which should be the case if the assumption leading to relation (8) were strictly valid. Note that in this region, the amplitude signal is no longer high pass filtered (the amplitude signal is "over its maximum", and this maximum defines the characteristic frequency $1/\tau_0$ of the feedback loop), which implies that the topographic data should be high pass filtered. However we observer no high-pass filtering of topography data in these data sets (compare this region of the PSD curves with the corresponding behaviour in **figure** 3). We attribute this non-standard behaviour to the fact that at these high temporal frequencies the SPM setup cannot be considered a simple (electronic) first order system defined only by the P/I values of the feedback loop. Instead, also mechanical resonances of the mechanical SPM setup and possibly even non-linearities of the tip-sample interaction have to be taken into account, rendering the tip sample system a much more complicated system in terms of transfer characteristic. In particular, we believe that for a faithful description of the tip–sample system orders higher than one, and possibly also non–linearities, have to be taken into account.

Finally, some additional practical issues not discussed so far should be emphasised. First, we note that for each SFM system the correct polarity of the error signal will have to be determined (what is seen low/high by the error signal?). This polarity determines the sign of relation (6),

that is, whether the error signal has to be added or subtracted (as assumed in the present work) in order to obtain the "true" topography. A second issue not discussed yet is the correct setpoint for image adquisition. In order for the error signal to faithfully reproduce the surface morphology, it has to be a linear function of tip-sample distance. Therefore the setpoint has to be chosen so that there is "enough signal" when passing over high and low surface features. This is illustrated in **figure 6** for the case of the oscillation amplitude as error signal. If possible, the setpoint i_0 of the interaction should be chosen such that the values between $i_0 - \delta z_{rms}$ and $i_0 + \delta z_{rms}$ depend linearly on the tip-sample distance (recall that the error signal is calibrated in length units), where δz_{rms} is the rms roughness of surface morphology. If the setpoint i_0 is chosen too close either to the free oscillation amplitude (a_{set}^b = bad setpoint in **figure 6**) or to the minimum amplitude needed to sustain a stable oscillation, then a small surface roughness will move the tip-sample system from the linear part of the amplitude vs distance curve. If this is the case, the error signal will not any more contain the correct information about the surface morphology, and the true surface morphology cannot be reconstructed as discussed in the present work.

6. DISCUSSION

We have shown that the correct determination of surface morphology using SPM techniques is extremely demanding and may be easily affected by experimental parameters. The description of surface morphology using PSD curves is a very powerful tool, but requires very good experimental raw data. In order to exploit the full potential of PSD analysis every experimental data point has to be a faithful representation of the true surface. For feedback based and sequential imaging techniques such as SPM, this is an very difficult task. The data shown here proves that in most cases if only topography data is acquired, the measured morphology is significantly affected by the feedback response of the SPM system. Then, the PSD curves calculated from this experimental data do not correspond to that of the true topography. Instead, either features are "lost" due to low pass filtering or features are "created" due to oscillation of the feedback loop. In most cases the PSD curves obtained from topographic images depend strongly on the parameters used for data adquisition (scan speed, P/I values of the feedback loop), and it is not clear which, if any, is the "good" curve. When the error signal of the feedback loop is acquired and analysed, the characteristic response time of the feedback loop can be determined. This response time determines, together with the scan speed, the maximum spatial frequency up to which the topographic data is measured faithfully. In addition, possible oscillation of the feedback loop can also be recognised

in the error signal. The error signal can thus be used to control the quality of the topographic image.

If the error signal is correctly calibrated (in length units: [nm]), then the topographic and the error signal can be summed (with the correct sign!) in order to give a "true" image that is a faithful representation of the surface morphology. In particular, this combined image does not depend on the particular set of parameters used for image adquisition. Interestingly, we observe that the best data is not acquired with high feedback parameters, since these result in oscillation of the feedback loop; imperceptible in the topographic and error signal data, but clearly observed in the corresponding PSD curves. Therefore for faithful imaging of the surface, the feedback parameters should not be pushed too high, instead, as discussed in this work, the calibrated error signal should be used to "recover" the small scale surface morphology, which is (low-pass) filtered by the feedback loop in the topographic image.

Since the nanoscale surface morphology determines many surface related processes such as friction, adhesion, wetting as well as many others, its correct determination is a fundamental issue in nanoscience. From a theoretical point of view, the PSD of surface topography is a basic tool to describe the statistical properties of surfaces and is used as a key parameter for the description of surface morphology in modern theories of friction and adhesion. Accordingly, its precise experimental measurement as proposed in this work is a fundamental issue for nanoscience, and we strongly believe that the approach presented in this work substantially improves the performance of any Scanning Force Microscope when using contact mode SFM as well as AM-DSFM, which are the two modes used for most imaging applications.

7. ACKNOWLEDGMENTS

---

[1] Bhushan, B. *"Modern Tribology Handbook"*. CRC Press, 2001.

[2] Persson, B., Albohr, O., Tartaglino, U., Volokitin, A. and Tosatti, E. *"On the nature of surface roughness with application to contact mechanics, sealing, rubber friction and adhesion"*. *Journal of Physics-Condensed Matter*, **volume 17(1)**:(2005) pp. R1–R62. doi:10.1088/0953-8984/17/1/R01.

[3] Zappone, B., Rosenberg, K. J. and Israelachvili, J. *"Role of nanometer roughness on the adhesion and friction of a rough polymer surface and a molecularly smooth mica surface"*. *Tribology Letters*, **volume 26(3)**:(2007) pp. 191–201. doi:10.1007/s11249-006-9172-y.

[4] Thomas, T. R. and Rosn, B. G. *"Determination of the optimum sampling interval for rough contact mechanics"*. *Tribology International*, **volume 33(9)**:(2000) pp. 601 – 610. doi:10.1016/S0301-679X(00)00076-1.

[5] Majumdar, A; Bhushan, B. *"Role of fractal geometry in roughness characterization and contact mechanics of surfaces"*. *Journal of Tribology-Transactions of the Asme*, **volume 112**:(1990) pp. 205–216.

[6] Heinrich G. *"Hysteresis friction of sliding rubbers on rough and fractal surfaces"*. *Rubber chemistry and technology*, **volume 70**:(1997) pp. 1–14.

[7] Ma, WL; Yang, CY; Heeger, AJ. *"Spatial Fourier-transform analysis of the morphology of bulk heterojunction materials used in "plastic" solar cells"*. *Advanced Materials*, **volume 19**:(2007) pp. 1387–1390. doi:10.1002/adma.200601933.

[8] Barthlott, W. and Neinhuis, C. *"Purity of the sacred lotus, or escape from contamination in biological surfaces"*. *Planta*, **volume 202(1)**:(1997) pp. 1–8.

[9] Flemming, M; Coriand, L; Duparré, A. *"Ultra-hydrophobicity through stochastic surface roughness"*. *Macromolecular Symposia*, **volume 23**:(2009) pp. 381–400.

[10] Flemming, M., Reihs, K. and Duparré, A. *"Characterization procedures for nanorough ultra-hydrophobic surfaces with controlled optical scatter"*. In Duparré, A and Singh, B, editor, *Advanced Characterization Techniques For Optics, Semiconductors, And Nanotechnologies*, volume 5188 of *Proceedings of the society of photo-optical instrumentation engineers (SPIE)*, pp. 246–253. SPIE, SPIE-INT SOC Optical Engineering, 1000 20TH ST, PO BOX 10, Bellingham, WA 98227-0010 USA, 2003. Conference on Advanced Characterization Techniques for Optics Semiconductors and Nanotechnologies, SAN DIEGO, CA, AUG 03-05, 2003.

[11] Watson, G. S., Cribb, B. W. and Watson, J. A. *How micro/nanoarchitecture facilitates anti-wetting: An elegant hierarchical design on the termite wing*. *ACS Nano*, **volume 4(1)**:(2010) pp. 129–136. PMID: 20099910, URL http://pubs.acs.org/doi/abs/10.1021/nn900869b.

[12] Stockman Y, Domken I, Hansen H, Tock JP, de Chambure D, Gondoin P. *"XMM flight mirror modules environmental and optical testing"*. *X-Ray Optics, Instruments and Missions*, **volume 3444**:(1998) pp. 302–312.

[13] Jianchao, C., Tao, S. and Jinghe, W. *"Comparison of optical surface roughness measured by stylus profiler, AFM and white light interferometer using power spectral density"*. In Zhang, Y and Sasian, JM and Xiang, L and To, S, editor, *5Th International Symposium On Advanced Optical Manufacturing And Testing Technologies: Optical Test And Measurement Technology And Equipment*, volume 7656 of *Proceedings of SPIE-The International Society for Optical Engineering*. COS-Chinese Opt Soc; SPIE, 2010.

[14] Wong, M; Eulenberger, J; Schenk, R, et al. *"Effect of surface-topology on the osseointegration of implant materials in trabecular bone"*. *Journal of Biomedical Materials Research*, **volume 29**:(1995) pp. 1567–1575.

[15] Alves, J. M., Brito, M. C., Serra, J. M. and Vallra, A. M. *A differential mechanical profilometer for thickness measurement*. *Review of Scientific Instruments*, **volume 75(12)**:(2004) pp. 5362–5363. URL http://dx.doi.org/doi/10.1063/1.1821627.

[16] Thomas, T. *Recent advances in the measurement and analysis of surface microgeometry*. *Wear*, **volume 33(2)**:(1975) pp. 205 – 233. URL http://www.sciencedirect.com/science/article/pii/004316487590277X.

[17] Elson, J. M. and Bennett, J. M. *"Calculation of the power spectral density from surface profile data"*. *Review of Scientific Instruments*, **volume 34(1)**:(1995) pp. 201–208.

[18] Duparré A., Ferre-Borrull J., Gliech S. et al. *"Surface characterization techniques for determining the root-mean-square roughness and power espectral densities of optical components"*. *Applied Physics*, **volume 41**:(2002) pp. 154–171.

[19] Binnig G., Rohrer H. *"Scanning tunneling microscopy"*. *Helvetica Physica Acta*, **volume 55**:(1982) pp. 726–735.

[20] Binnig G., Quate C.F. and Gerber Ch. *"Atomic Force Microscope"*. *Phys. Rev. Letter*, **volume 56**:(1986) pp. 930–933. doi:10.1103/PhysRevLett.56.930.

[21] Gómez Rodríguez J M, Baró A M, Salvarezza R C. *"Fractal Characterization Of Gold Deposits By Scanning Tunneling Microscopy"*. *Journal of Vacuum Science & Technology B*, **volume 9**:(1991)

pp. 495–499.

[22] Gómez Rodríguez J M, Baró A M, Vázquez L, Salvarezza R C, Vara J M, Arvia A J. *"Fractal surfaces of gold and platinum electrodeposits - dimensionality determination by scanning tunneling microscopy". Journal of Physical Chemistry*, **volume 96**:(1992) pp. 347–350.

[23] Ferr-Borrull, J., Steinert, J. and Duparr, A. *Extending the capabilities of scanning probe microscopy for microroughness analysis in surface engineering. Surface and Interface Analysis*, **volume 33(2)**:(2002) pp. 92–95. URL <http://dx.doi.org/10.1002/sia.1169>.

[24] Hartmann E, Hahn P O, Behm R J. *"Determination of nanometer structures and surface-roughness of polished Si wafers by Scanning Tunneling Microscopy". J. Appl. Physics*, **volume 69**:(2005) pp. 4273–4281.

[25] Sandra E Fritz, Tommie Wilson Kelley and C. Daniel Frisbie. *"Effect of dielectric roughness on performance of pentacene TFTs and Restoration of performance with a polymeric smoothing layer". Journal of Physical Chemistry B*, **volume 109**:(2005) pp. 10574–10577.

[26] Fang, S., Haplepete, S., Chen, W., Helms, C. and Edwards, H. *"Analyzing atomic force microscopy images using spectral methods". Journal of Applied Physics*, **volume 82(12)**:(1997) pp. 5891–5898.

[27] Ruffino, F., Grimaldi, M. G., Giannazzo, F., Roccaforte, F. and Raineri, V. *"Atomic Force Microscopy Study of the Kinetic Roughening in Nanostructured Gold Films on SiO_2". Nanoscale Research Letters*, **volume 4(3)**:(2009) pp. 262–268. doi:10.1007/s11671-008-9235-0.

[28] Meyers, G. F., Dineen, M. T., Shaffer II, E. O., Stokich Jr., T. and Im, J.-h. *"Characterization of the surface structural, mechanical, and thermal properties of benzocyclobutene dielectric polymers using scanned probe microscopy". Macromolecular Symposia*, **volume 167(1)**:(2001) pp. 213–226. doi:10.1002/1521-3900(200103)167:1⟨213::AID-MASY213⟩3.0.CO;2-D.

[29] Liu, F., Li, C., Zhu, M., Gu, J. and Zhou, Y. *"Kinetic roughening and mound surface growth in microcrystalline silicon thin films"*. In Schropp, REI, editor, *Physica Status Solidi C - Current Topics In Solid State Physics, Vol 7 No 3-4*, volume 7 of *Physica Status Solidi C-Current Topics in Solid State Physics*, pp. 533–536. Wiley-V C H Verlag GMBH, Pappelallee 3, W-69469 Weinheim, Germany, 2010. doi:10.1002/pssc.200982734. 23rd International Conference on Amorphous and Nanocrystalline Semiconductors (ICANS23), Utrecht, Netherlands, AUG 23-28, 2009.

[30] Inés Nieto Carvajal et. al. To be published.

[31] Nanotec Electrónica. *E-28760, Tres Cantos*. For more information see www.nanotec.es.

[32] Olympus Optical Co. LDT. Olympus Cantilevers, long cantilever (length $240\mu m$, width $30\mu m$, OMCL-RC series AC240TS). For more information see www.olympus.co.jp/probe.

[33] Juan Francisco González Martínez et. al, 2011. In preparation.

[34] Colchero, J., Cuenca, M., González Martínez, J. F., Abad, J., Perez Garcia, B., Palacios-Lidon, E. and Abellán, J. *Thermal frequency noise in dynamic scanning force microscopy. Journal Of Applied Physics*, **volume 109(2)**. doi:10.1063/1.3533769.

[35] Horcas, I., Fernández, R., Gómez-Rodríguez, J. M., Colchero, J., Gómez-Herrero, J. and Baró, A. M. *"WSXM: A software for scanning probe microscopy and a tool for nanotechnology". Review of Scientific Instruments*, **volume 78(1)**. doi:10.1063/1.2432410.

[36] Palacios-Lidon, E. Munuera, C. Ocal and Colchero, J. *"Contrast inversion in non-contact Dynamic Scanning Force Microscopy: What is high and what is low?". Ultramicroscopy*, **volume 110(7)**:(2010) pp. 789–800. doi:10.1016/ultramic.2010.01.015.

[37] Note that even for a sharp surface feature the SPM images would be smoothened due to tip convolution, that is the sharp surface feature would "see" the curvature of the tip.

[38] Probably the wider peak in the first graph has the same origin but is observed wider and at lower frequencies due to aliasing.

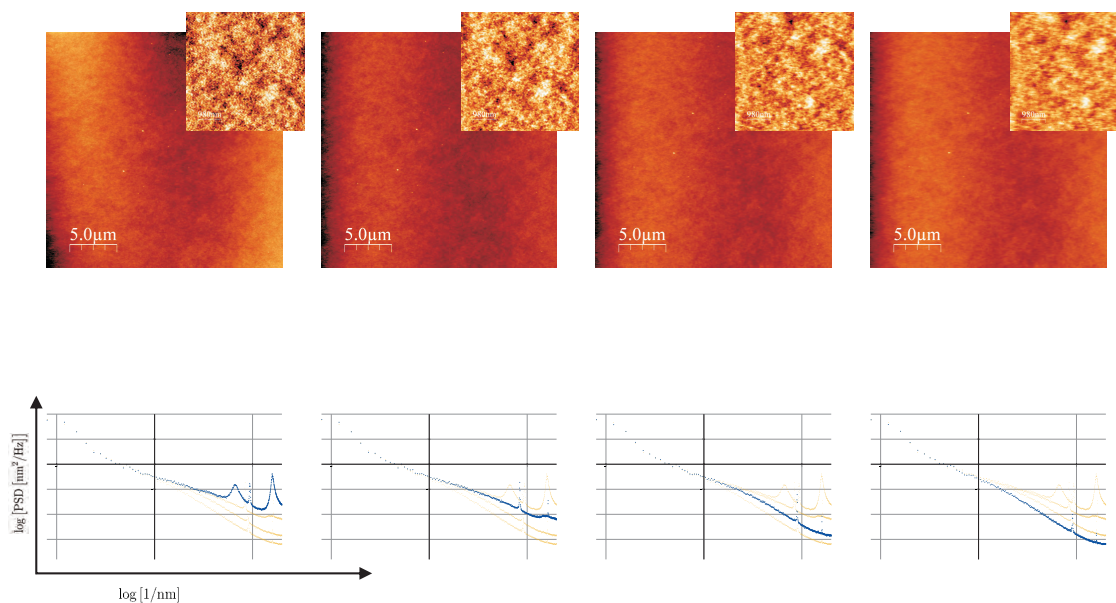## 8. FIGURE CAPTIONS

8.1. Figure 1

Figure 1

Top row: Topography images of the surface of a commercial glass cover slide acquired at a scan frequency of 1 line/s, but at different settings for the feedback loop. Feedback response was decreased from left to right: proportional/integral parameters are 125/25, 80/16, 40/8 and 20/4 (in arbitrary units). Image size is 1024×1024 and the total acquisition time was about 18 minutes. The insets shows enlarged regions of each topographic image with an amplified grey scale. Lower row: graphs of the PSD curves of surface roughness calculated from the corresponding (large scale) topographic image. Lateral size of the larger images is 25 μm, smaller images show a zoom of 5 μm. The total grey scale of all large scale images is 8 nm and 1 nm for all insets. Bottom row: PSD curves calculated from the topographic images; the graphs show the logarithm of the PSD of surface roughness plotted versus the logarithm of the inverse length scale. For each graph the thinner yellow lines show the PSD curves of all the other images, while the thicker blue line shows the PSD curve for the correspondent topographic image shown in the same column. The grid lines for the PSD graphs are $\Delta \log[\kappa] = 1$ (horizontal axis) and $\Delta \log[\mathrm{PSD}] = 1$ (vertical axis).

19

8.2. Figure 2

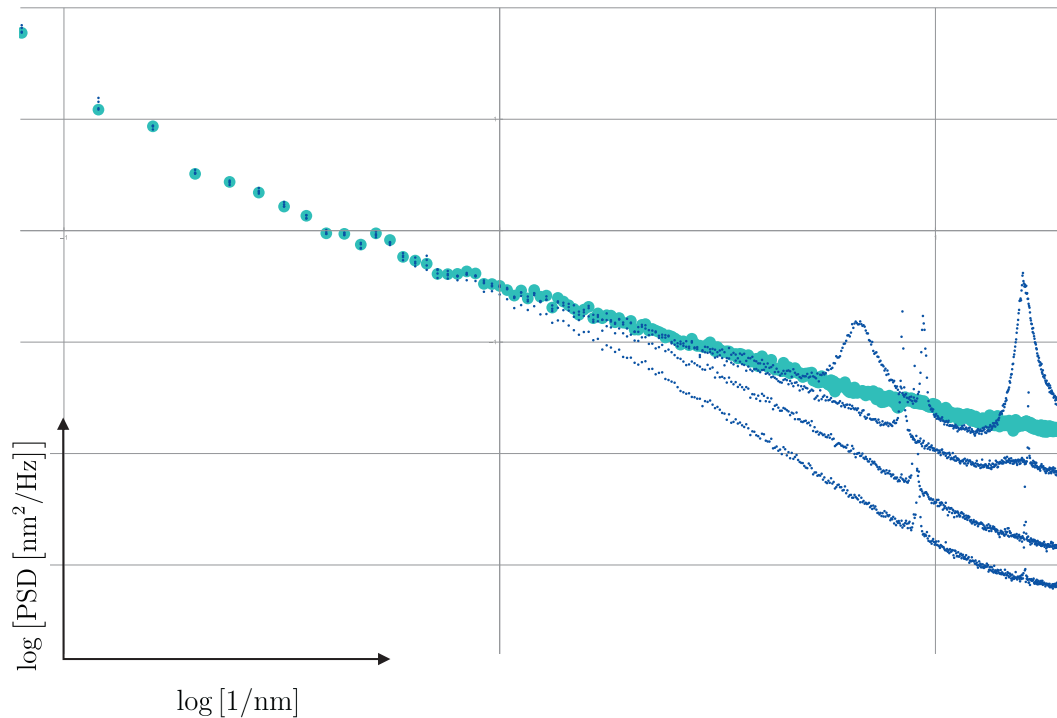
Figure 2

PSD curves calculated from the topographic images shown in **figure 1** as well as from the discussion above.The graphs show the logarithm of the PSD of surface roughness plotted versus the logarithm of the inverse length scale. The thinner lines correspond to the PSD curves of the individual images shown in **figure 1**, the thicker line to a master curve described in the main text. The grid lines for the PSD graphs are $\Delta \log[\kappa] = 1$ (horizontal axis) and $\Delta \log[\text{PSD}] = 1$ (vertical axis).

8.3. Figure 3

Images of a Platinum surface taken all at a scan frequency of 1 line/s, but at different settings for the feedback loop (from left to right: 90/45, 45/22.5, 15/7.5, 5/2.5, 1/0.5). The images and graphs in the same column correspond to a common data set, since the corresponding images have been acquired simultaneously at a fixed values of the feedback loop. The upper row shows topographic images, the middle row amplitude images and the lower row graphs of the PSD curves of surface roughness. In each graph, the PSD of surface roughness has been calculated for the
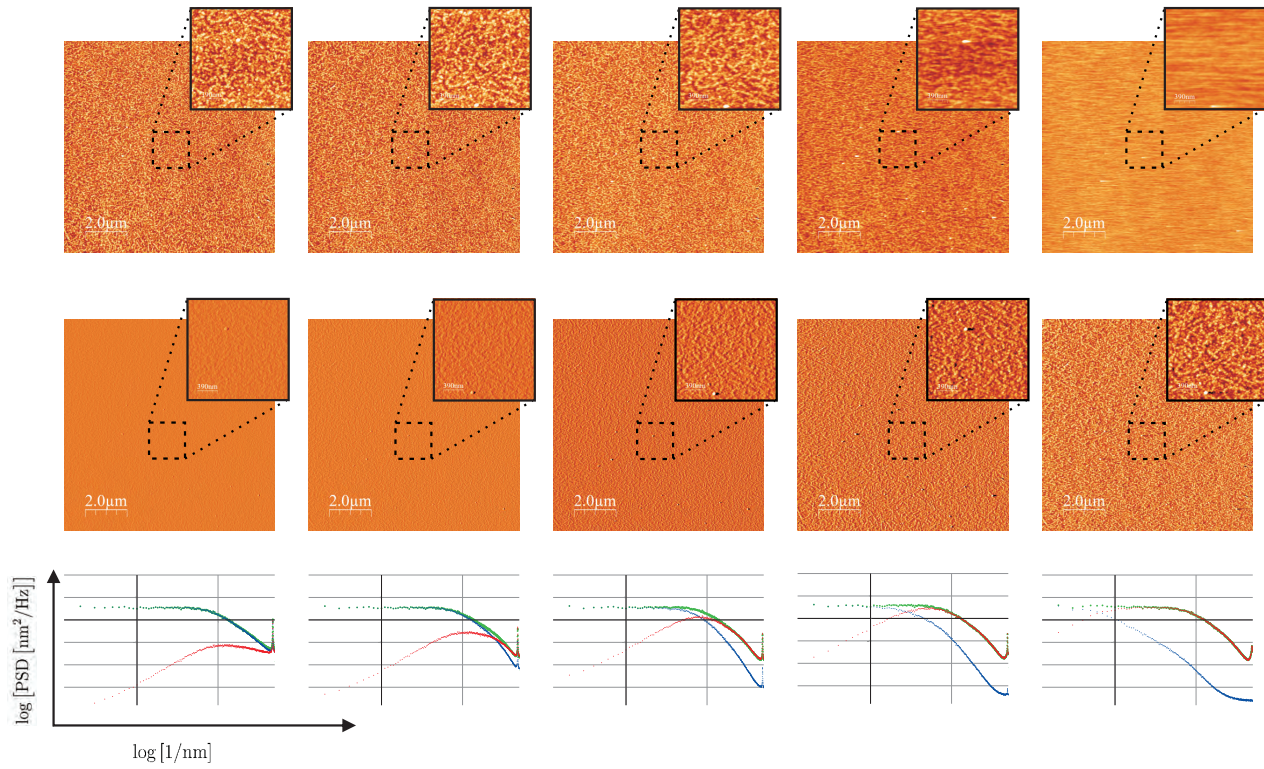
20

Figure 3

topography and amplitude image shown in the corresponding column, as well as for the difference $z_{\text{true}} = z_{\text{fb}} - \Delta I_{\text{err}}$ (corresponding image not shown). Lateral size of the larger images is 10 μm, smaller images show a zoom of 1 μm. The total grey scale of all images is 5 nm (large and small scale images as well as topographic and amplitude images). Lower row: PSD curves calculated from the topography and amplitude images as well as the difference data (image not shown). The grid lines for the PSD graphs are $\Delta \log[\kappa] = 1$ (horizontal axis) and $\Delta \log[\text{PSD}] = 1$ (vertical axis). Green lines correspond to the PSD curves of topography plus error signal, blue curves to the topography and red curves to the error signal.

8.4. Figure 4

PSD curves corresponding to the topography and amplitude images shown in **figure 3** as well as of the difference data. Each graph shows the $\log(\text{PSD}[1/\lambda])$ vs $\log(1/\lambda)$ curve for the data acquired at different P/I values. While the different curves are clearly distinguished in the topography (a) and amplitude (b) PSDs, the curves corresponding to the difference (c) essentially fall on the same "master curve". The grid lines for the PSD graphs are $\Delta \log[\kappa] = 1$ (horizontal axis) and $\Delta \log[\text{PSD}] = 1$ (vertical axis).
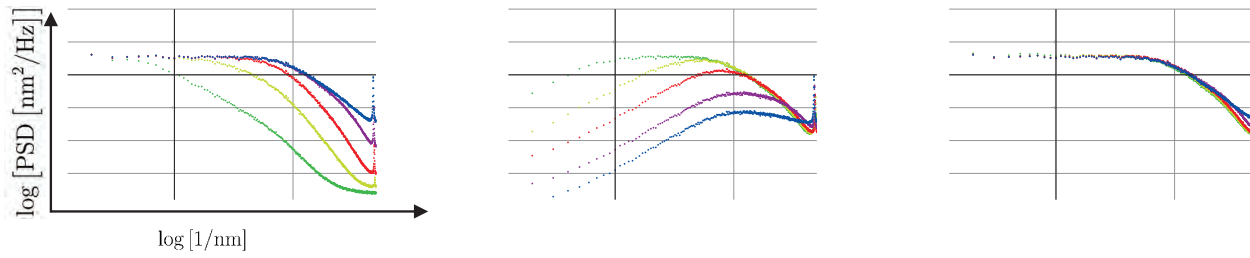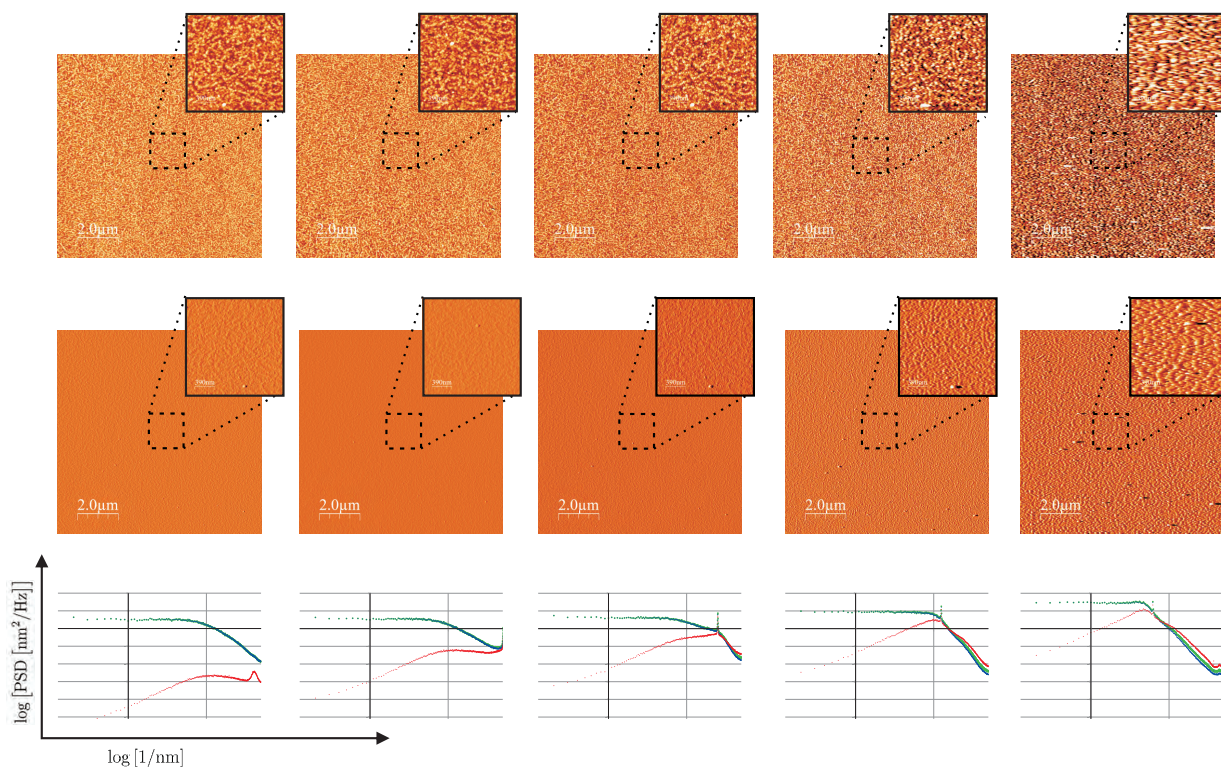
21

Figure 4

8.5. Figure 5

Figure 5

Images of the same Platinum film as shown in **figure 3**. The images shown were acquired at the same value of the feedback loop, but at different imaging speeds (from left to right: 0.5, 1, 2, 4, 8 lines/s). As previously the upper row shows topographic images, the middle row amplitude images and the lower row graphs of the corresponding PSD curves of surface roughness. Again, lateral size of the larger images is 10 μm, smaller images show a zoom of 1 μm. The total grey scale of all images is 5 nm. The grid lines for the PSD graphs are $\Delta \log[\kappa] = 1$ (horizontal axis)

and $\Delta \log[\text{PSD}] = 1$ (vertical axis).
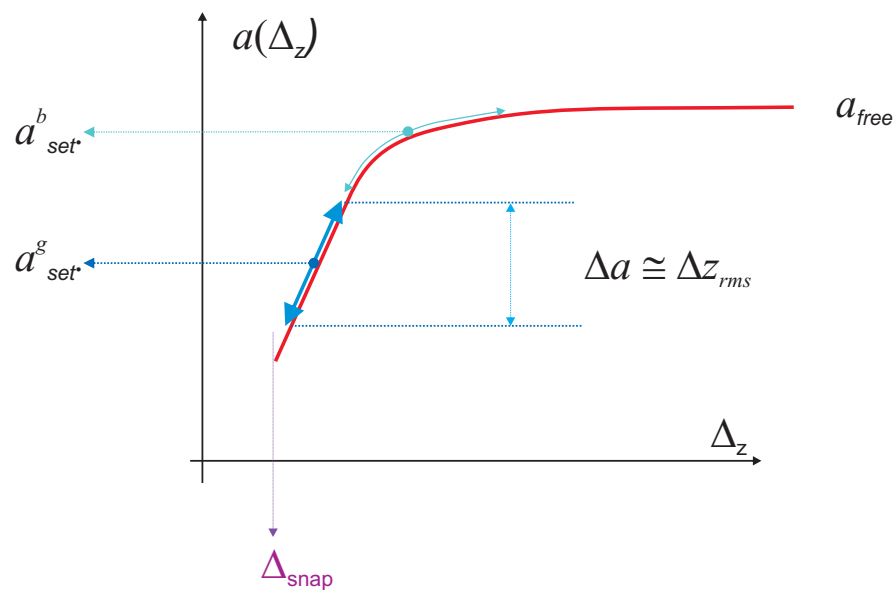
8.6. Figure 6

Figure 6

Schematic representation of the oscillation amplitude vs the tip-sample distance. For large tip sample distances, the free oscillation amplitude is measured. As the oscillating tip interacts with the surface the oscillation decreases linearly with tip sample distance. For small oscillation amplitude, the energy pumped into the cantilever by the external driving circuit is not sufficient to compensate for the losses induced by the tip-sample interaction, and the oscillation stops. If the feedback loop does not respond instantaneously to height variations as the tip is scanned over the surface, height variations will result in variations of the oscillation amplitude. For the kind of applications proposed in this work, the tip-sample system has to stay in the linear regime of the amplitude vs distance curve.